Journal of Materials Chemistry C

PAPER

View Article Online
View Journal | View Issue

Cite this: J. Mater. Chem. C, 2014, 2, 4581

Design of liquid crystals with 'de Vries-like' properties: carbosilane-terminated 5-phenylpyrimidine mesogens suitable for chevron-free FLC formulations†

Christopher P. J. Schubert,[a] Andreas Bogner,[b] Jan H. Porada,[b] Khurshid Ayub,[a] Tamer Andrea,[a] Frank Giesselmann[b] and Robert P. Lemieux*[a]

Received 27th February 2014
Accepted 15th April 2014

DOI: 10.1039/c4tc00393d

www.rsc.org/MaterialsC

Smectic liquid crystals with 'de Vries-like' properties are characterized by a maximum layer contraction of ≤1% upon transition from the orthogonal SmA phase to the tilted SmC phase. In an effort to expand the library of 'de Vries-like' liquid crystals required for the formulation of chevron-free ferroelectric liquid crystal mixtures, we report the synthesis of a homologous series of tricarbosilane 5-phenylpyrimidine liquid crystals **QL16-*n*** using an improved synthetic route, and the characterization of their liquid crystalline and 'de Vries-like' properties. Measurements of orientational order parameters S_2 and effective molecular lengths L_{eff} by monodomain 2D X-ray scattering suggest that 'de Vries-like' behavior in series **QL16-*n*** is due to the combined effect of an increase in S_2 and a decrease in bilayer interdigitation, thus causing a smectic layer expansion that compensates for the molecular tilt in the SmC phase. We also show how the optical tilt angle in the SmC phase may be optimized for SSFLC displays—without compromising 'de Vries-like' properties—by shortening the tricarbosilane end-group to a dicarbosilane. Two of the new materials reported herein, 5-[4-(12,12,14,14,16,16-hexamethyl-12,14,16-trisilaheptadecyloxy)phenyl]-2-hexyloxypyrimidine (**QL16-6**) and 2-hexyloxy-5-[4-(12,12,14,14-tetramethyl-12,14-disilapentadecyloxy)phenyl]pyrimidine (**QL24-6**) rank among the best 'de Vries-like' materials reported heretofore, with broad SmC phases and reduction factors R of 0.17 and 0.18, respectively, at a reduced temperature $T - T_{AC} = -10$ K. We also show that inverting the orientation of the 5-phenylpyrimidine core in the homologous series **QL17-*n*** causes a suppression of 'de Vries-like' properties. These results suggest that non-covalent core–core interactions in the intercalated smectic bilayers formed by these mesogens may influence 'de Vries-like' behavior.

Introduction

Ferroelectric liquid crystals are macroscopically polar fluids formed by rod-shaped mesogens that self-organize into a chiral smectic C* (SmC*) mesophase, which is characterized by a diffuse layer structure with a period d corresponding to the layer spacing, a uniform tilt of the director **n** with respect to the layer normal **z**, and a helical structure caused by the precession of **n** about **z** from layer to layer (Fig. 1). Alignment of a SmC* liquid crystal between glass slides with a rubbed alignment substrate (*e.g.*, polyimide) causes the unwinding of the SmC* helix into a surface-stabilized configuration with a spontaneous polarization P_S oriented perpendicular to the glass slides.[1–3] By coupling P_S to an electric field, this surface-stabilized ferroelectric liquid crystal (SSFLC) film can be switched between opposite tilt orientations to give an electro-optical shutter between crossed polarizers that is currently used in high-resolution reflective color microdisplays.

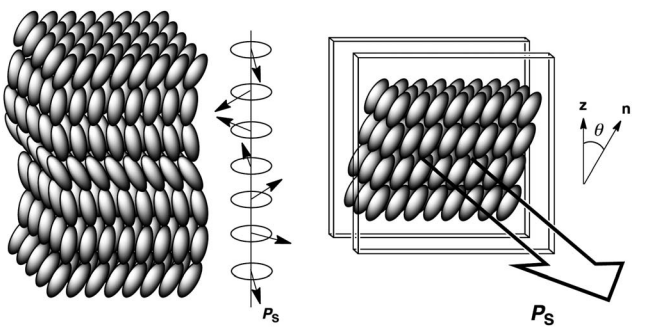

Fig. 1 Schematic representation of hard spherocylinders forming a SmC* phase in the absence of boundary conditions (left), and as a surface-stabilized ferroelectric liquid crystal film in a bookshelf geometry (right).

[a]Chemistry Department, Queen's University, Kingston, Ontario, Canada. E-mail: lemieux@chem.queensu.ca

[b]Institute of Physical Chemistry, Universität Stuttgart, Pfaffenwaldring 55, D-70569 Stuttgart, Germany

† Electronic supplementary information (ESI) available: Detailed experimental and synthetic procedures. See DOI: 10.1039/c4tc00393d

The formulation of liquid crystal mixtures for SSFLC display applications requires diverse libraries of chiral and achiral materials in order to optimize a wide range of physical parameters, including temperature range, Goldstone mode viscosity, optical tilt angle, birefringence, helical pitch and spontaneous polarization.[3] Another key requirement that has yet to be achieved in commercial mixtures, and which has limited the commercialization of SSFLC technology beyond microdisplay applications, is the formation of a chevron-free bookshelf geometry in the SmC* phase. In conventional FLC mixtures, a high quality alignment in ITO glass cells with rubbed polyimide layers is achieved by cooling from the chiral nematic (N*) phase to the SmC* phase *via* the orthogonal SmA* phase. However, the layer contraction of ~7–10% that typically occurs upon cooling from the SmA* to the SmC* phase results in buckling of the smectic layers from a bistable bookshelf geometry into a chevron geometry because of surface anchoring;[4] the formation of chevrons with opposite fold directions results in zigzag line defects that severely degrade the optical quality of the SSFLC film.

'De Vries-like' liquid crystals present a unique solution to the chevron geometry problem.[5] These are smectic liquid crystals characterized by a maximum layer contraction of ≤1% on cooling from the orthogonal SmA phase to the tilted SmC phase. This unusual behavior was first explained by de Vries using a 'diffuse cone' model in which mesogens in the SmA phase have a tilted orientation and a degenerate azimuthal distribution,[6] although more recent theoretical work suggests that 'de Vries-like' behavior may result from an unusual combination of high lamellar order and low orientational order.[5,7–9] This is consistent with the fact that most 'de Vries-like' mesogens feature nanosegregating elements such as a trisiloxane end-group or a perfluorinated side-chain that strongly promote lamellar ordering. Chiral 'de Vries-like' liquid crystals tend to have unusually large electroclinic tilt susceptibilities, with the field-induced electroclinic tilt accompanied by a significant increase in birefringence and minimal contraction of the smectic layer spacing.[5] The electro-optical behavior of two such materials with first-order SmA*–SmC* transitions was recently explained using a generalized Langevin-Debye model, which assumes a random azimuthal distribution of molecules on a fixed tilt cone of angle θ, with an orientational distribution in which the tilt θ is allowed to vary with the applied field over a prescribed range.[10]

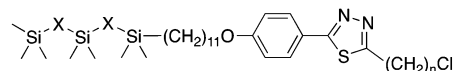

QL5-*n*: X=O
QL6-*n*: X=CH_2

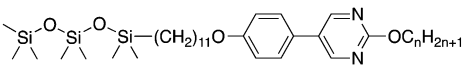

QL15-*n*

To expand the library of 'de Vries-like' liquid crystals for the formulation of chevron-free FLC mixtures, we developed a strategy based on designing mesogenic structures that combine a nanosegregating end-group with a SmA-promoting element. For example, the organosiloxane and carbosilane 2-phenylthiadiazole derivatives **QL5-6** and **QL6-6**, and the organosiloxane 5-phenylpyrimidine derivative **QL15-5** undergo a SmA–SmC transition with a maximum layer contraction of only 0.4–0.5%.[11,12] These three materials have reduction factors R ranging from 0.20 to 0.24 at 10 K below the SmA–SmC transition temperature T_{AC}, which are comparable to those calculated for the best 'de Vries-like' materials reported previously.[13,14] The reduction factor R (eqn (1)) is a measure of 'de Vries-like' character defined as the ratio of the tilt angle $\delta(T)$ required to give a layer contraction $d_C(T)/d_{AC}$ at a temperature T below T_{AC}, assuming a conventional model of hard spherocylinders, over the tilt angle θ_{opt} measured experimentally by polarized optical microscopy.[15] According to eqn (1), a SmA–SmC transition would approach that described by the diffuse cone model of de Vries as R approaches 0.

$$R = \delta(T)/\theta_{opt}(T) = \cos^{-1}[d_C(T)/d_{AC}]/\theta_{opt}(T) \quad (1)$$

The profiles of relative layer spacing d/d_{AC} *vs.* reduced temperature $T - T_{AC}$ exhibited by these materials typically show a pronounced negative thermal expansion in the SmA phase that persists on cooling into the SmC phase and counteracts the layer contraction caused by tilting to such an extent that the layer spacing at the SmA–SmC transition is eventually restored, as shown in Fig. 2. Recent analyses by 2D X-ray scattering of smectic monodomains formed by 'de Vries-like' organosiloxane liquid crystals similar to **QL5-6** have shown that they exhibit unusually large molecular tilt fluctuations, and that the layer contraction due to molecular tilt upon SmA–SmC transition is almost fully compensated by an increase in the orientational order parameter S_2 as tilt fluctuations decrease with decreasing temperature.[16] On the other hand, similar analyses of monodomains formed by the 5-phenylpyrimidine derivatives **QL15-4** and **QL15-9** show that S_2 is almost invariant of temperature in both SmA and SmC phases, and that the layer contraction due to molecular tilt is compensated primarily by an increase in effective molecular length L_{eff}.[17] This may be interpreted as a change in the degree of interdigitation in smectic bilayers formed by these materials (*vide infra*).

Trisiloxane end-groups are known to promote the lamellar ordering of calamitic mesogens due to the tendency of siloxane and hydrocarbon segments to nanosegregate into

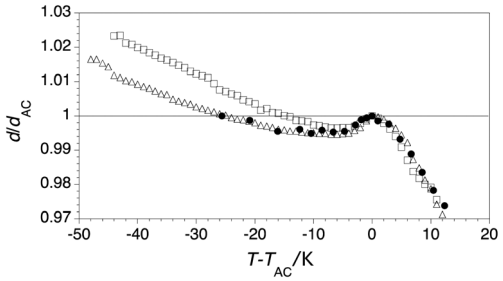

Fig. 2 Relative smectic layer spacing d/d_{AC} *vs.* reduced temperature $T - T_{AC}$ for compounds **QL5-6** (△), **QL6-6** (□) and **QL15-5** (●). From ref. 11 and 12.

distinct sub-layers, which results in the formation of partially intercalated smectic bilayers.[18] Organosiloxane mesogens are known to form very stable SmC phases, which may be due to a suppression of out-of-layer fluctuations that reduces the entropic cost of molecular tilt. In the design of mesogens such as **QL5-6**, 'de Vries-like' behavior was achieved by combining a trisiloxane end-group as SmC-promoting element with a chloro-terminated alkyl chain as SmA-promoting element.[12,19] Likewise, in the design of mesogens such as **QL15-5**, 'de Vries-like' behavior was achieved by combining a trisiloxane end-group with a 5-phenylpyrimidine core, which is also a strong SmA-promoting element.[11,20,21]

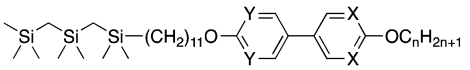

QL16-*n*: X=N, Y=CH
QL17-*n*: X=CH, Y=N

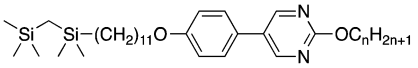

QL24-*n*

To address the hydrolytic instability of siloxanes, which precludes their use in liquid crystal display applications, Reddy *et al.* showed that a chemically inert tricarbosilane can be substituted for a trisiloxane as the nanosegregating element of a smectic mesogen.[22] We recently carried out a similar substitution in mesogens such as **QL5-*n*** to give **QL6-*n*** without significantly affecting their mesogenic or 'de Vries-like' properties.[12] In this paper, we report the synthesis of a homologous series of carbosilane 5-phenylpyrimidine derivatives **QL16-*n*** using an improved synthetic route, and the characterization of their mesogenic and 'de Vries-like' properties. We also report on the effect of inverting the orientation of the 5-phenylpyrimidine core in the homologous series **QL17-*n*** (hereinafter called the 'inverted' series), which suggests that non-covalent core–core interactions in the intercalated bilayers formed by these mesogens influence 'de Vries-like' behavior. Finally, we show how the optical tilt angle in these materials may be optimized for use in SSFLC devices—without compromising 'de Vries-like' properties—by shortening the tricarbosilane end-group to a dicarbosilane, as in **QL24-6**.

Results and discussion

Synthesis

The synthetic route originally reported for the organosiloxanes **QL15-*n*** includes a rather inefficient deprotection step in which a methoxy group is selectively demethylated in the presence of the *n*-alkoxy chain using NaSEt.[11] In the improved synthetic route shown in Scheme 1, the THP-protected phenylboronic acid **1** is coupled to 5-bromo-2-chloropyrimidine (**2**) under Suzuki–Miyaura conditions to give **3**, which is subjected to nucleophilic aromatic substitution with the appropriate sodium alkoxide, and deprotected upon acidic workup to give the 2-alkoxy-5-(4-hydroxyphenyl)pyrimidine **4(*n*)**. The mesogens **QL16-*n*** are then obtained by alkylation of **4(*n*)** with 1-bromo-12,12,14,14,16,16-hexamethyl-12,14,16-trisilaheptadecane. The mesogen **QL24-6** is similarly obtained by alkylation with 1-bromo-12,12,14,14-tetramethyl-12,14-disilapentadecane. The inverted mesogens **QL17-*n*** are obtained by deprotection of **3** and alkylation with the appropriate alkyl bromide to give **6(*n*)**, followed by nucleophilic aromatic substitution with 12,12,14,14,16,16-hexamethyl-12,14,16-trisilaheptadecan-1-ol and NaH.

Mesogenic properties

The mesophases formed by compounds **QL16-*n*** and **QL17-*n*** (Table 1) were characterized by polarized optical microscopy (POM) and differential scanning calorimetry (DSC). With one exception (**QL16-9**), all compounds form enantiotropic SmA and SmC phases, as shown by the characteristic fan and homeotropic textures of the SmA phase that turn into broken fan and Schlieren textures, respectively, upon transition to the SmC phase. Substituting the tricarbosilane end-group in **QL16-6** with a dicarbosilane end-group to give **QL24-6** resulted in a 17 K increase in melting point, but the SmC and SmA temperature ranges remained approximately the same on heating. A higher order smectic phase appeared on cooling below the SmC phase, which was identified as a SmF phase based on the characteristic change of the Schlieren texture into a mosaic texture, as shown in Fig. 3.[23]

In all compounds investigated, texture analyses revealed a significant change in interference color on cooling from the isotropic phase to the SmC phase under polarized optical microscopy (see the fan textures in Fig. 3a and b, for example). We recorded the interference color change in the fan textures formed by a 10 μm film of **QL16-6**, which showed a blue-green color in the SmA phase that is almost invariant of temperature, but then sharply changed to a green-yellow color upon transition to the SmC phase and gradually turned to orange at 10 K below T_{AC} (see Fig. S1a in ESI†). The overall color change corresponds to an increase in birefringence $\Delta\Delta n$ of *ca.* 0.02, according to a Michel-Levy chart, which is consistent with that previously observed for the 'de Vries-like' material 3M 8422,[5] and is indicative of an increase in orientational order.[5,12] The apparent discontinuity in birefringence at the SmA–SmC transition is also consistent with discontinuities in $S_2(T)$ observed at the SmA–SmC transition of 'de Vries-like' materials.[16,17] A similar change in birefringence was observed with a 10 μm film of **QL17-6** (see Fig. S1b in ESI†).

As shown in Fig. 4, increasing the length of the alkoxy chain in the two homologous series results in a gradual decrease in the temperature range of the SmA phase, which is consistent with empirical trends. A comparison of phase transition temperatures for **QL15-*n*** and **QL16-*n*** shows that substituting the trisiloxane end-group with a tricarbosilane causes a decrease in both clearing and SmA–SmC transition temperatures, whereas the variations in melting temperatures are more random; the homologue **QL16-6** forms a particularly broad SmC phase, with a melting point approaching room temperature. Furthermore, shortening the tricarbosilane end-group in **QL16-6** to a dicarbosilane causes the melting point to rise by 17 K,

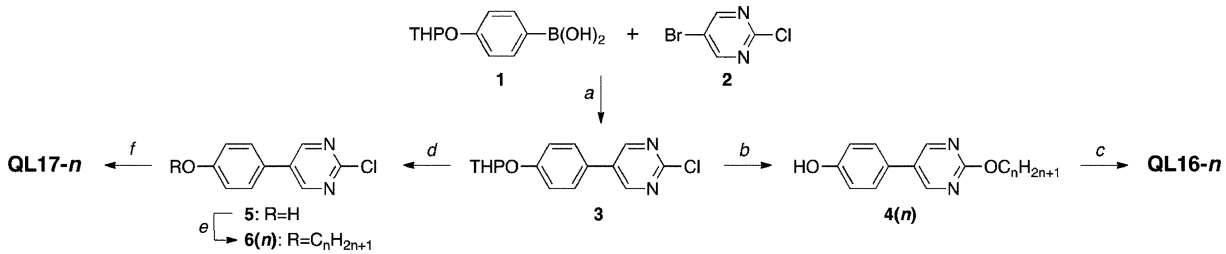

Scheme 1 Reagents and conditions: (a) $Pd_2(dba)_3$, Cy_3P, K_3PO_4, 1,4-dioxane, 76%; (b) (i) $C_nH_{2n+1}OH$, NaH, THF; (ii) H_3O^+, 70–80%; (c) 1-bromo-12,12,14,14,16,16-hexamethyl-12,14,16-trisilaheptadecane, Cs_2CO_3, acetone, 85–95%; (d) TsOH, 1 : 1 CH_2Cl_2–EtOH, 99%; (e) $C_nH_{2n+1}Br$, Cs_2CO_3, acetone, 75–90%; (f) 12,12,14,14,16,16-hexamethyl-12,14,16-trisilaheptadecan-1-ol, NaH, THF, 60–70%.

Table 1 Transition temperatures (°C) and enthalpies of transitions (kJ mol^{-1}, in parentheses) for compounds **QL16-*n***, **QL17-*n*** and **QL24-6** on heating

Compound	Cr	Cr′	SmF	SmC	SmA	*I*
QL16-4	• 43 (20)			• 44 (<0.1)[a]	• 68 (8.2)	•
QL16-5	• 34	• 40 (21)[b]		• 55 (<0.1)[a]	• 66 (7.5)	•
QL16-6	• 33 (22)			• 64 (<0.1)[a]	• 69 (7.8)	•
QL16-7	• 64 (33)			• 65[c]	• 67 (3.7)	•
QL16-8	• 58 (37)			• 66 (0.9)	• 68 (6.6)	•
QL16-9	• 67 (66)			(• 65 (1.2))[d]	(• 66 (6.0))[d]	•
QL17-4	• 39 (20)			• 42 (<0.1)[a]	• 68 (7.6)	•
QL17-5	• 44 (22)			• 48 (<0.1)[a]	• 66 (6.2)	•
QL17-6	• 48 (23)			• 59 (<0.1)[a]	• 72 (9.4)	•
QL17-7	• 51 (26)			• 61 (<0.1)[a]	• 70 (8.0)	•
QL17-8	• 56 (27)			• 63 (0.2)	• 70 (8.8)	•
QL17-9	• 57	• 60 (30)[b]		• 63 (0.3)	• 69 (8.5)	•
QL24-6	• 50 (31)		(• 42 (1.9))[d]	• 78 (<0.1)[a]	• 81 (11)	•

[a] Transition temperature measured by polarized microscopy. [b] Total enthalpy for both transitions due to partial resolution of the peaks. [c] Cr–SmC and SmC–SmA peaks overlap. [d] Monotropic mesophase.

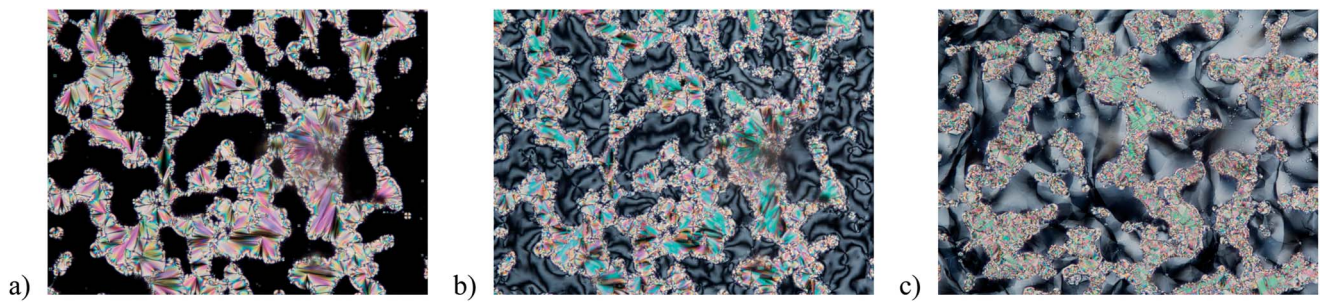

Fig. 3 Polarized photomicrographs of **QL24-6** (a) at 80 °C in the SmA phase, (b) at 77 °C in the SmC phase and (c) at 43 °C in the SmF phase.

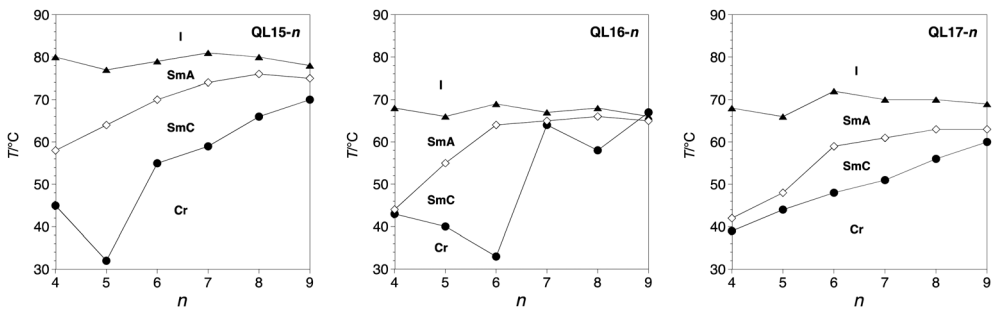

Fig. 4 Phase transition temperatures as a function of the chain length *n* in the homologous series **QL15-*n*** (from ref. 11*a*), **QL16-*n*** and **QL17-*n***: melting point (●), SmC–SmA transition (◇), SmA–isotropic transition (▲).

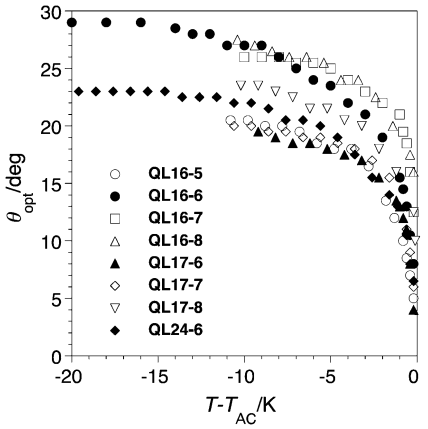

Fig. 5 Optical tilt angle θ_{opt} *vs.* reduced temperature $T - T_{AC}$ measured on cooling for selected homologues in series **QL16-*n***, **QL17-*n***, and for compound **QL24-6**; the filled symbols correspond to the three homologues with $n = 6$.

which is consistent with a previous report on organosiloxane liquid crystals by Naciri *et al.*[18d] Inverting the core orientation in **QL17-*n*** has little effect on the clearing temperature, which is more or less invariant of chain length, or the SmA–SmC transition temperature. However, the melting temperature shows a more regular increase with the alkoxy chain length, with no evidence of any odd-even effect.

Optical tilt angles (θ_{opt}) were measured by POM as a function of reduced temperature $T - T_{AC}$ in the absence of an electric field for those materials that form a SmC phase with a relatively broad temperature range on heating and/or cooling.[24] As shown in Fig. 5, the tilt angle increases with increasing alkyl chain length in both homologous series, which is consistent with empirical trends.[11] A comparison of tilt angles formed by the three homologues with $n = 6$, shown as filled symbols in Fig. 5, highlights two significant structure–property relationships: (i) shortening the tricarbosilane end-group to a dicarbosilane causes a reduction in θ_{opt}, which may be due to a weakening of the nanosegregation imposed by the carbosilane end-group; and (ii) inverting the core orientation also causes a reduction in θ_{opt} that is even more substantial than that caused by a shortening of the carbosilane end-group. However, substituting the trisiloxane end-group with a tricarbosilane has relatively little effect on tilt angle (*e.g.*, 31° *vs.* 30° at saturation for **QL15-6** and **QL16-6**, respectively).[11] From a formulation perspective, the tilt angle of 23° formed by **QL24-6** at saturation is near the ideal θ_{opt} value of 22.5° required for maximum contrast in a SSFLC electro-optical device.[3]

Small angle X-ray scattering

Accurate measurements of the smectic layer spacing d as a function of temperature were carried out by small angle X-ray scattering (SAXS). The measurements were performed on heating from the crystalline phase except for compound **QL16-7**, which was analyzed on cooling from the isotropic liquid phase. As shown in Fig. 6a, the profiles of relative layer spacing d/d_{AC} *vs.* reduced temperature $T - T_{AC}$ for selected homologues in series **QL16-*n*** and for **QL24-6** show the characteristics of 'de Vries-like' materials, *i.e.*, a negative thermal expansion of d in the SmA phase that persists in the SmC phase and compensates for the layer contraction due to tilt. The shorter homologues **QL16-5**, **QL16-6** and **QL24-6** show maximum layer contractions $\%lc_{max}$ of only 0.4–0.5%; the longer homologues **QL16-7** and **QL16-8** have $\%lc_{max}$ of 0.8–1.0%, which may be explained by the higher tilt angles formed in the SmC phase. Indeed, the calculated reduction factors R at $T - T_{AC} = -10$ K show relatively little difference in 'de Vries-like' properties between these five

Table 2 Maximum layer contraction $\%lc_{max}$, optical tilt angle θ_{opt} and reduction factor R at $T - T_{AC} = -10$ K for compounds **QL16-*n***, **QL17-*n*** and **QL24-6**

Compound	$\%lc_{max}$	θ_{opt}/°	R
QL16-5	0.4	20	0.21
QL16-6	0.5	27	0.17
QL16-7	1.0	26	0.24
QL16-8	0.8	26	0.20[a]
QL17-6	1.5	20	0.49
QL17-7	1.9	20	0.56
QL17-8	1.4	22	0.44[b]
QL24-6	0.4	22	0.18

[a] At $T - T_{AC} = -7$ K. [b] At $T - T_{AC} = -6$ K.

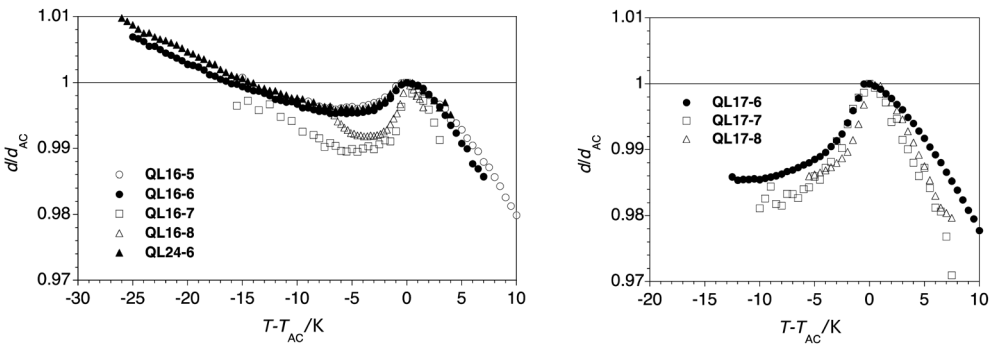

Fig. 6 Relative smectic layer spacing d/d_{AC} *vs.* reduced temperature $T - T_{AC}$ for (a) selected homologues in series **QL16-*n*** and for **QL24-6**, and (b) for selected homologues in series **QL17-*n***; the filled symbols correspond to the three homologues with $n = 6$. The data for **QL16-7** were acquired on cooling from the isotropic liquid phase.

compounds; overall, the compounds **QL16-6** and **QL24-6**, rank among the best 'de Vries-like' materials reported heretofore (Table 2).[11–14]

Remarkably, the inversion of core orientation in series **QL17-*n*** has a detrimental effect on 'de Vries-like' properties. As shown in Fig. 6b, the d/d_{AC} *vs.* $T - T_{AC}$ profiles for the inverted homologues **QL17-6**, **QL17-7** and **QL17-8** show the expected negative thermal expansion of d in the SmA phase, but it does not persist in the SmC phase to the extent that the layer contraction due to molecular tilt is compensated. Maximum layer contractions for these compounds range from 1.5% to 1.9%, which is still well below the 7–10% range exhibited by conventional smectogens. However, with optical tilt angles that are significantly smaller than those formed by the **QL16-*n*** isomers, the R values for the inverted isomers **QL17-*n*** turn out to be about twice as large, ranging from 0.44 to 0.56. It is also worth noting that the layer spacing d_{AC} for the material with the best R value, **QL16-6**, is *ca.* 2.2 Å shorter than for the inverted isomer **QL17-6**, which may be ascribed to a difference in S_2, but also to a difference in degree of interdigitation in the bilayer structure (*vide infra*).

Monodomain 2D X-ray scattering

In order to understand the difference in 'de Vries-like' properties between the two isomeric series **QL16-*n*** and **QL17-*n***, we carried out X-ray scattering analyses on smectic monodomains formed by the representative isomers **QL16-6** and **QL17-6**. Two-dimensional X-ray scattering patterns were obtained as a function of temperature from smectic monodomains, which allowed simultaneous measurements of the director tilt θ, the layer spacing d, and the orientational order parameter S_2.[16,17] The latter is a measure of the orientational order about the director **n** according to eqn (2), where β is the angle formed by the long axis of a single molecule and the director **n**, which represents the average direction of all long molecular axes. The effective molecular length L_{eff} is derived from S_2, d and θ according to eqn (3).[16] X-ray scattering patterns obtained with **QL16-6** in the SmA and SmC phases are shown in Fig. 7 as representative examples.

$$S_2 = 0.5\langle 3\cos^2\beta - 1\rangle \quad (2)$$

$$d(T) = 1/3L_{eff}(S_2(T) + 2)\cos\theta(T) \quad (3)$$

The inner small-angle scattering corresponding to the periodicity along the layer normal **z** shows a sharp fundamental and two higher-order Bragg peaks, which is indicative of a high lamellar order. There are two wide-angle scattering maxima with varying intensities over the azimuthal angle χ, as shown by the decomposition into two $I(q)$ profiles in Fig. 8a, which are consistent with a nanosegregation of the carbosilane segments from the hydrocarbon segments. The assignment of the inner wide-angle scattering to the carbosilane sub-layer was confirmed by a 2D X-ray scattering analysis of 2,2,4,4,6-pentamethyl-2,4,6-trisilaheptane,[25] which produced an $I(q)$ profile of the isotropic scattering that matches perfectly the first fitted peak of **QL16-6** (see Fig. 8b). The inner wide-angle scattering is much broader in χ than the outer wide-angle scattering corresponding to the hydrocarbon sub-layer, which indicates that the carbosilane end-groups have a much lower orientational order; a similar observation was made with respect to the siloxane end-groups in **QL15-4** and **QL15-9**.[17] In the SmA phase, the diffuse wide-angle maxima are perpendicular to the layer peaks and rotate in the same direction by an angle θ upon cooling into the SmC phase; the absence of bimodal broadening of the wide-angle intensity profile along χ at the SmA–SmC transition indicates that the incident X-ray beam is probing a well-aligned smectic monodomain.

To measure S_2 and θ, the wide-angle intensity profile $I(\chi)$ was obtained by integrating the intensity I scattered along the

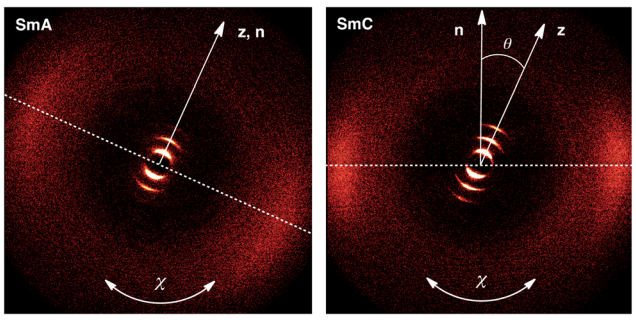

Fig. 7 2D X-ray scattering patterns from a smectic monodomain formed by **QL16-6** in the SmA phase at 72 °C and in the SmC phase at 42 °C. The director **n** is orthogonal to the dotted line joining the centers of the diffuse wide angle scattering and makes an angle θ with layer normal **z** in the SmC phase.

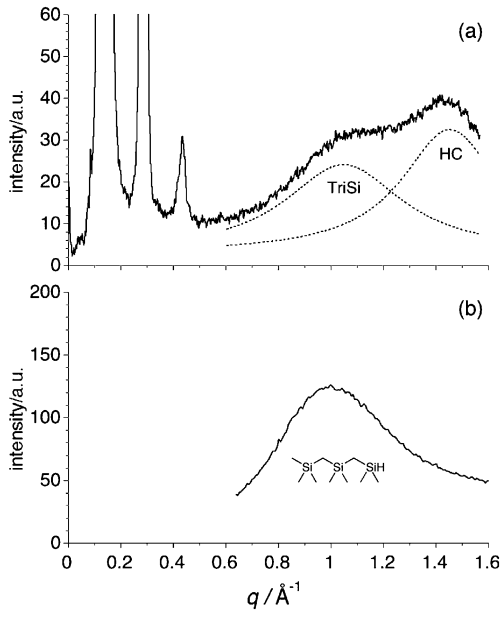

Fig. 8 Intensity profiles of the X-ray scattering vector q for (a) **QL16-6** in the SmC phase at 42 °C, and (b) for 2,2,4,4,6-pentamethyl-2,4,6-trisilaheptane in the isotropic liquid phase at 40 °C. The dotted curves represent the Lorentz fits to the measured data for the tricarbosilane scattering (TriSi) and the hydrocarbon scattering (HC).

azimuthal angle χ over the range of q, including both the inner carbosilane and the outer hydrocarbon rings. Values of θ were obtained from the shift in the $I(\chi)$ maxima in χ (see Fig. 7); values of S_2 were obtained by analyzing the $I(\chi)$ profile according to the method of Davidson *et al.*[26,27] As $I(\chi)$ contains all contributions from the carbosilane and hydrocarbon segments, the resulting values of θ and S_2 represent averages taken over the entire molecule.

As shown in Fig. 9c, S_2 for **QL16-6** is relatively invariant of temperature in the SmA phase, and the approximate value of 0.48 is significantly lower than S_2 values typical of a conventional SmA phase (0.7–0.8);[28] S_2 increases with decreasing temperature in the SmC phase to a maximum value of 0.63. The $S_2(T)$ profile for **QL17-6** is not significantly different, although S_2 values are slightly higher and increase with decreasing temperature through both the SmA and SmC phases, from 0.42 to 0.63. Both $S_2(T)$ profiles show a discontinuity at the SmA–SmC transition, which is consistent with the corresponding interference color change observed in the texture analysis of both compounds. The significant difference between the two isomers lies in the effective length profiles $L_{\text{eff}}(T)$. In the case of **QL16-6**, L_{eff} increases with decreasing temperature, from 51.6 to 54.0 Å, which is consistent with a decrease in bilayer interdigitation; in the case of **QL17-6**, L_{eff} shows relatively little variance with temperature, ranging from 54.1 to 54.8 Å. In both cases, L_{eff} values exceed the length of 41.3 Å for a fully extended molecular model minimized at the B3LYP/6-31G* level (see Fig. S2 in ESI†), which is consistent with an intercalated bilayer structure.

We illustrate the relative contributions of changes in S_2 and L_{eff} to the $d(T)$ profiles of **QL16-6** and **QL17-6** by deconstructing the profiles using eqn (3), as shown in Fig. 10. Assuming, in the borderline case of a conventional SmA–SmC transition, that S_2 and L_{eff} remain constant,[5,9] one can calculate the $d(T)$ profiles due only to changes in molecular tilt θ by inserting into eqn (3) the values of S_2 and L_{eff} at the SmA–SmC transition point T_{AC} as constants (see the lower curves (○) in Fig. 10). By inserting the variable $S_2(T)$ into eqn (3) and keeping L_{eff} constant, one obtains the middle curves (△), which both show a partial compensation of layer contraction due to the increase in orientational ordering. The top curves (●) correspond to the experimental $d(T)$ profiles and include contributions from both $S_2(T)$ and $L_{\text{eff}}(T)$. Hence, this analysis suggests that 'de Vries-like' behavior in **QL16-6** is due, at a first approximation, to the combined effect of an increase in orientational order and a decrease in bilayer interdigitation on a nearly equal basis. In the case of **QL17-6**, the analysis suggests that the increase in orientational order does counteract to some extent the layer contraction due to molecular tilt, but is not enough to produce the effect observed with **QL16-6** due to the relatively small variance in bilayer interdigitation.

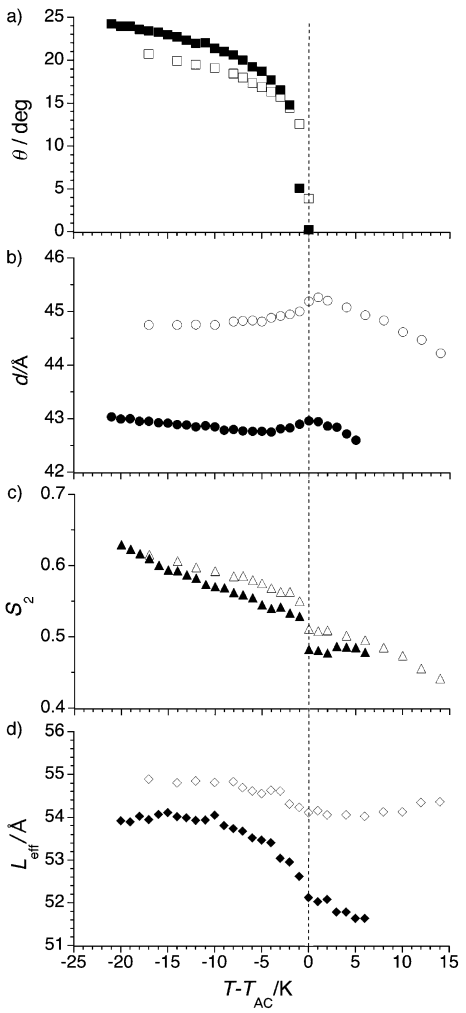

Fig. 9 Temperature dependence of (a) the director tilt angle θ, (b) the layer spacing d, (c) the orientational order parameter S_2, and (d) the effective molecular length L_{eff} for **QL16-6** (filled symbols) and **QL17-6** (open symbols).

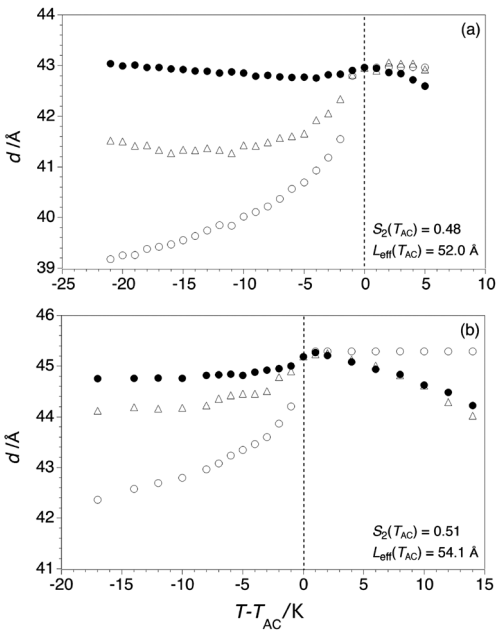

Fig. 10 Smectic layer spacing d *vs.* reduced temperature $T - T_{\text{AC}}$ derived from eqn (3) with experimental values of θ for (a) **QL16-6** and (b) **QL17-6**: (○) including S_2 and L_{eff} = constants at T_{AC}; (△) including $S_2(T)$, L_{eff} = constant at T_{AC}; (●) including $S_2(T)$, $L_{\text{eff}}(T)$.

Conclusions

The results presented herein are consistent with our previous report that substitution of a trisiloxane end-group with a chemically inert tricarbosilane end-group in 'de Vries-like' liquid crystals does not significantly affect mesogenic or 'de Vries-like' properties. This work also expands our library of *bona fide* 'de Vries-like' mesogens with broad SmC phases that may be useful in the formulation of chevron-free FLC mixtures, and shows that the tilt angle of these materials may be adjusted by shortening the tricarbosilane end-group without compromising 'de Vries-like' behavior.

Furthermore, the effect of core inversion on the reduction factor R in the homologous series **QL17-*n*** provides new insight in our investigation of the origins of 'de Vries-like' properties in these materials. The $S_2(T)$ profiles resulting from the monodomain X-ray scattering experiments suggest that core inversion has relatively little effect on orientational order in both SmA and SmC phases, and that an increase in S_2 with decreasing temperature partially counteracts the layer contraction due to molecular tilt upon transition from the SmA to the SmC phase in both homologous series **QL16-*n*** and **QL17-*n***. However, the results of this study suggest that 'de Vries-like' behavior is only achieved when the increase in S_2 is combined with a concomitant decrease in bilayer interdigitation. These findings differ from previous X-ray diffraction studies of siloxane-terminated mesogens suggesting that 'de Vries-like' behavior is due to *either* a variance in orientational order *or* a variance in bilayer interdigitation.[16,17] Indeed, one can conclude from this and previous studies that there may be a continuum of complementary effects giving rise to 'de Vries-like' behavior. The difference in $L_{\mathrm{eff}}(T)$ between **QL16-6** and the inverted isomer **QL17-6** suggests that the decrease in bilayer interdigitation on cooling **QL16-6** from the SmA to the SmC phase may be driven by a minimization of antiparallel core–core interaction potential that may already be achieved in the intercalated bilayer formed by **QL17-6** in the SmA phase. To test this hypothesis, we are carrying out a detailed modeling study of the bilayer structure formed by these mesogens; the results of this study will be reported in due course.

Acknowledgements

We thank the Natural Sciences and Engineering Research Council of Canada (Discovery and CREATE grants) and the Deutsche Forchungsgemeinschaft (NSF/DFG Materials World Network program DFG Gi 243/6) for support of this work.

References

1 N. A. Clark and S. T. Lagerwall, *Appl. Phys. Lett.*, 1980, **36**, 899–901.
2 *Ferroelectric Liquid Crystals: Principles, Properties and Applications*, ed. J. W. Goodby, R. Blinc, N. A. Clark, S. T. Lagerwall, M. A. Osipov, S. A. Pikin, T. Sakurai, K. Yoshino and B. Zeks, Gordon & Breach, Philadelphia, 1991.
3 S. T. Lagerwall, *Ferroelectric and Antiferroelectric Liquid Crystals*, Wiley-VCH, Weinheim, 1999.
4 T. P. Rieker, N. A. Clark, G. S. Smith, D. S. Parmar, E. B. Sirota and C. R. Safinya, *Phys. Rev. Lett.*, 1987, **59**, 2658–2661.
5 For a review, see: J. P. F. Lagerwall and F. Giesselmann, *ChemPhysChem*, 2006, **7**, 20–45.
6 A. de Vries, *J. Chem. Phys.*, 1979, **71**, 25–31.
7 M. V. Gorkunov, M. A. Osipov, J. P. F. Lagerwall and F. Giesselmann, *Phys. Rev. E: Stat., Nonlinear, Soft Matter Phys.*, 2007, **76**, 051706.
8 K. Saunders, D. Hernandez, S. Pearson and J. Toner, *Phys. Rev. Lett.*, 2007, **98**, 197801.
9 S. T. Lagerwall, P. Rudquist and F. Giesselmann, *Mol. Cryst. Liq. Cryst.*, 2009, **510**, 148–157.
10 Y. Shen, L. Wang, R. Shao, T. Gong, C. Zhu, H. Yang, J. E. Maclennan, D. M. Walba and N. A. Clark, *Phys. Rev. E: Stat., Nonlinear, Soft Matter Phys.*, 2013, **88**, 062504.
11 (*a*) J. C. Roberts, N. Kapernaum, Q. Song, D. Nonnenmacher, K. Ayub, F. Giesselmann and R. P. Lemieux, *J. Am. Chem. Soc.*, 2010, **132**, 364–370; (*b*) J. C. Roberts, N. Kapernaum, F. Giesselmann and R. P. Lemieux, *J. Am. Chem. Soc.*, 2008, **130**, 13842–13843.
12 (*a*) Q. Song, D. Nonnenmacher, F. Giesselmann and R. P. Lemieux, *J. Mater. Chem. C*, 2013, **1**, 343–350; (*b*) Q. Song, D. Nonnenmacher, F. Giesselmann and R. P. Lemieux, *Chem. Commun.*, 2011, **47**, 4781–4783.
13 M. D. Radcliffe, M. L. Brostrom, K. A. Epstein, A. G. Rappaport, B. N. Thomas, R. Shao and N. A. Clark, *Liq. Cryst.*, 1999, **26**, 789–794.
14 M. S. Spector, P. A. Heiney, J. Naciri, B. T. Weslowski, D. B. Holt and R. Shashidhar, *Phys. Rev. E: Stat. Phys., Plasmas, Fluids, Relat. Interdiscip. Top.*, 2000, **61**, 1579–1584.
15 Y. Takanishi, Y. Ouchi, H. Takezoe, A. Fukuda, A. Mochizuki and M. Nakatsuka, *Jpn. J. Appl. Phys., Part 1*, 1990, **2**, L984–L986.
16 D. Nonnenmacher, S. Jagiella, Q. Song, R. P. Lemieux and F. Giesselmann, *ChemPhysChem*, 2013, **14**, 2990–2995.
17 H. Yoon, D. M. Agra-Kooijman, K. Ayub, R. P. Lemieux and S. Kumar, *Phys. Rev. Lett.*, 2011, **106**, 087801.
18 (*a*) H. J. Coles, H. Owen, J. Newton and P. Hodge, *Liq. Cryst.*, 1993, **15**, 739–744; (*b*) K. Sunohara, K. Takatoh and M. Sakamoto, *Liq. Cryst.*, 1993, **13**, 283–294; (*c*) H. Poths, E. Wischerhoff, R. Zentel, A. Schönfeld, G. Henn and F. Kremer, *Liq. Cryst.*, 1995, **18**, 811–818; (*d*) J. Naciri, J. Ruth, G. Crawford, R. Shashidhar and B. R. Ratna, *Chem. Mater.*, 1995, **7**, 1397–1402; (*e*) J. Z. Vlahakis, K. E. Maly and R. P. Lemieux, *J. Mater. Chem.*, 2001, **11**, 2459–2464.
19 I. Rupar, K. M. Mulligan, J. C. Roberts, D. Nonnenmacher, F. Giesselmann and R. P. Lemieux, *J. Mater. Chem. C*, 2013, **1**, 3729–3735.
20 The model compound 5-(4-butyloxyphenyl)-2-octyloxypyrimidine forms only a SmA phase (Cr 84 SmA 117 I). T. Hegmann, M. R. Meadows, M. D. Wand and R. P. Lemieux, *J. Mater. Chem.*, 2004, **14**, 185–190.
21 R. Pecheanu and N. M. Cann, *Phys. Rev. E: Stat., Nonlinear, Soft Matter Phys.*, 2010, **81**, 041704.

22 R. A. Reddy, C. Zhu, R. Shao, E. Korblova, T. Gong, Y. Shen, E. Garcia, M. A. Glaser, J. E. Maclennan, D. M. Walba and N. A. Clark, *Science*, 2011, **332**, 72–77.
23 I. Dierking, *Textures of Liquid Crystals*, Wiley-VCH, Weinheim, 2003.
24 The advantages of this method over measuring θ_{opt} by electro-optical switching in the SmC* phase are that (i) no doping with a chiral additive is required, and (ii) there are no possible contribution from an electroclinic effect near T_{AC}. P. Rudquist, private communication.
25 Y. Zhang, U. Baumeister, C. Tschierske, M. J. O'Callaghan and C. Walker, *Chem. Mater.*, 2010, **22**, 2869–2884.
26 P. Davidson, D. Petermann and A.-M. Levelut, *J. Phys. II*, 1995, **5**, 113–131.
27 F. Giesselmann, R. Germer and A. Saipa, *J. Chem. Phys.*, 2005, **123**, 034906.
28 A. J. Leadbetter and E. K. Norris, *Mol. Phys.*, 1979, **38**, 669–686.